BIOCHEMISTRY
including biophysical chemistry & molecular biology

ARTICLE

pubs.acs.org/biochemistry

Two Distinct Ferritin-like Molecules in *Pseudomonas aeruginosa*: The Product of the *bfrA* Gene Is a Bacterial Ferritin (FtnA) and Not a Bacterioferritin (Bfr)

Huili Yao,[†] Grace Jepkorir,[†] Scott Lovell,[‡] Pavithra V. Nama,[†] Saroja Weeratunga,[†] Kevin P. Battaile,[§] and Mario Rivera*[,†]

[†]Ralph N. Adams Institute for Bioanalytical Chemistry and Department of Chemistry, University of Kansas, Multidisciplinary Research Building, 2030 Becker Drive, Lawrence, Kansas 66047, United States

[‡]Del Shankel Structural Biology Center, University of Kansas, 2034 Becker Drive, Lawrence, Kansas 66047, United States

[§]IMCA-CAT, Hauptman Woodward Medical Research Institute, Sector 17, Advanced Photon Source, Argonne National Laboratory, 9700 South Cass Avenue, Building 435A, Argonne, Illinois 60439, United States

Supporting Information

ABSTRACT: Two distinct types of ferritin-like molecules often coexist in bacteria, the heme binding bacterioferritins (Bfr) and the non-heme binding bacterial ferritins (Ftn). The early isolation of a ferritin-like molecule from *Pseudomonas aeruginosa* suggested the possibility of a bacterioferritin assembled from two different subunits [Moore, G. R., et al. (1994) *Biochem. J. 304*, 493−497]. Subsequent studies demonstrated the presence of two genes encoding ferritin-like molecules in *P. aeruginosa*, designated *bfrA* and *bfrB*, and suggested that two distinct bacterioferritins may coexist [Ma, J.-F., et al. (1999) *J. Bacteriol. 181*, 3730−3742]. In this report, we present structural evidence demonstrating that the product of the *bfrA* gene is a ferritin-like molecule not capable of binding heme that harbors a catalytically active ferroxidase center with structural properties similar to those characteristic of bacterial and archaeal Ftns and clearly distinct from those of the ferroxidase center typical of Bfrs. Consequently, the product of the *bfrA* gene in *P. aeruginosa* is a bacterial ferritin, which we propose should be termed *Pa* FtnA. These results, together with the previous characterization of the product of the *bfrB* gene as a genuine bacterioferritin (*Pa* BfrB) [Weeratunga, S. J., et al. (2010) *Biochemistry 49*, 1160−1175], indicate the coexistence of a bacterial ferritin (*Pa* FtnA) and a bacterioferritin (*Pa* BfrB) in *P. aeruginosa*. In agreement with this idea, we also obtained evidence demonstrating that release of iron from *Pa* BfrB and *Pa* FtnA is likely subject to different regulation in *P. aerugionsa*. Whereas the efficient release of iron stored in Pa FtnA requires only the input of electrons from a ferredoxin NADP reductase (*Pa* Fpr), the release of iron stored in *Pa* BfrB requires not only electron delivery by *Pa* Fpr but also the presence of a "regulator", the apo form of a bacterioferritin-associated ferredoxin (apo *Pa* Bfd). Finally, structural analysis of iron uptake *in crystallo* suggests a possible pathway for the internalization of ferroxidase iron into the interior cavity of *Pa* FtnA.

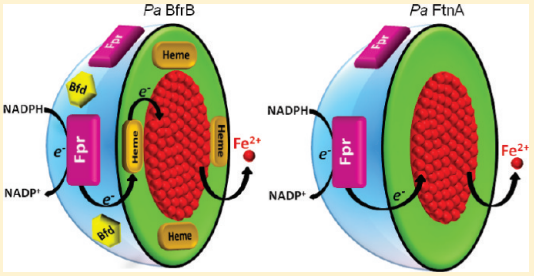

Bacteria have developed several strategies for acquiring and managing iron that include (1) deployment of molecules with high affinity for iron or heme to scavenge iron from the surroundings,[1−4] (2) storage of intracellular iron to provide a source of the nutrient when external supplies become limited,[5−7] (3) employment of redox stress resistance systems to minimize damage caused by iron-induced reactive oxygen species,[8,9] and (4) appropriate regulation of the expression of iron-binding proteins to meet the availability of iron.[10] In *Pseudomonas aeruginosa* and in many other pathogens, these events are regulated by Fur, the master Fe uptake regulator,[11] and by regulatory small RNAs.[12] Significant advances have improved our understanding of the process of uptake of iron and heme-iron by *P. aeruginosa* and other pathogens.[13−18] In comparison, how the cell allows the utilization of its intracellular iron while avoiding iron toxicity remains to be understood. One mechanism whereby iron toxicity can be ameliorated or controlled is the storage of excess iron in ferritin and ferritin-like molecules. These molecules function by oxidizing Fe^{2+} using O_2 and H_2O_2 as electron acceptors and internalize the resultant Fe^{3+} in the form of a mineral. When environmental iron concentrations are low, Fe^{3+} stored in ferritin-like molecules is mobilized for its incorporation in metabolism, which is why ferritin-like molecules act as dynamic regulators of cytosolic iron concentrations.

Ferritin-like molecules are found in eukaryotes and prokaryotes.[6] Eukaryotic ferritins are composed of two different

Received: March 19, 2011
Revised: May 13, 2011
Published: May 16, 2011

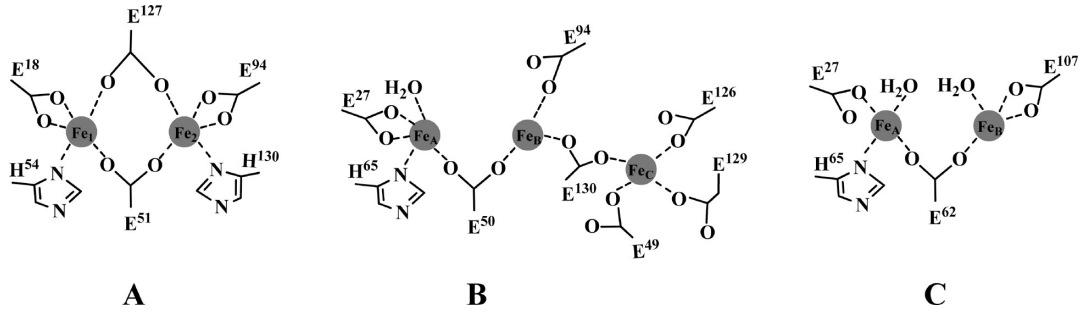

Figure 1. Schematic representation of the (A) symmetrical ferroxidase center typical of bacterioferritin (Bfr) where Fe_1 and Fe_2 are bridged by two Glu residues (numbering as in *Pa* BfrB), (B) ferroxidase center seen in *E. coli* and archaeal Ftn (see the text) [site C (Fe_C) is included in addition to ferroxidase iron Fe_A and Fe_B and numbering as in *Ec* FtnA], and (C) ferroxidase center of human H-ferritin adapted from the crystal structure of its Tb^{3+} derivative.[56]

but isostructural subunit types, H and L, which assemble into a 24-mer structure.[19] In comparison, two types of ferritin-like molecules can be found in bacteria, the ferritins (Ftn) and the bacterioferritins (Bfr).[5,6] Ftns are composed of 24 subunits that assemble into a spherical protein shell surrounding a central cavity in which the iron mineral is stored. Each subunit consists of a four-helix bundle and a short C′-terminal helix that is nearly perpendicular to the axis of the bundle. The hollow interior of ferritin-like molecules provides a large cavity for the storage of iron in the form of a ferric mineral, which can consist of as many as ~4500 iron atoms. The protein cage keeps the ferric mineral soluble and appears to isolate it from participating in redox reactions that may cause oxidative stress. A hallmark of the bacterioferritin structure is the presence of heme groups.[20,21] In all bacterioferritins of known structure, each heme is located on a 2-fold symmetric axis within a subunit dimer, where it is axially coordinated by M^{52} from each subunit. Hence, 12 subunit dimers assemble to form the Bfr structure containing 12 heme molecules. The heme iron plays a key role in mediating the passing of electrons across the protein coat to reduce the ferric iron mineral, prior to its release for incorporation in metabolism.[22]

Ferritin-like molecules take soluble Fe^{2+} and store it as a ferric (Fe^{3+}) mineral, which means that the iron storage process requires a ferroxidation step. This process is catalyzed by specific sites in the protein called ferroxidase centers, which in bacterial Ftn and in Bfr are located in the middle of each subunit.[23] Despite the central role played by the ferroxidase center in the process of iron uptake, its structure is not conserved among eukaryotic ferritins, bacterial ferritins, and bacterioferritins. Available structures, however, suggest significant structural conservation of ferroxidase centers among Ftns and among Bfrs. The main structural differences among ferroxidase centers in eukaryotic Ftn, Bfr, and bacterial Ftn are illustrated in Figure 1. The ferroxidase center of Bfr is highly symmetrical,[24−28] with each of the iron ions (Fe_1 and Fe_2) coordinated by two bridging glutamates and by His and Glu residues as capping ligands (Figure 1A). In the ferroxidase center of bacterial and archaeal Ftns of known structure, Fe_A and Fe_B are bridged by only one protein-provided ligand[29−32] (Figure 1B). In this context, the ferroxidase center of bacterial Ftns is more similar to the ferroxidase center of eukaryotic Ftns (Figure 1C) than to the ferroxidase center of Bfrs. An interesting feature of bacterial Ftn is the presence of an additional iron near the ferroxidase center.[29] This site, also observed in the ferroxidase center of *Pyrococcus furiosus*[31] and *Archaeoglobus fulgidus*[32] ferritins, has been termed "site C" and is not essential for iron mineralization but appears to exert an influence in the process of moving iron into the protein cavity.[21,33]

Early studies reported that bacterioferritin isolated from *P. aeruginosa* seemed to be heterogeneous and consist of two types of subunits, α and β, which were found to be present in different proportions, depending on the sample.[34,35] Subsequent investigations established two genes encoding ferritin-like molecules in *P. aeruginosa*, termed *bfrA* and *bfrB*,[9] under the assumption that they encode two bacterioferritins, BfrA and BfrB. An amino acid sequence alignment comparing the amino acid sequence of the protein encoded by the *bfrA* gene with those corresponding to bacterioferritins of known structure (Figure S1 of the Supporting Information) shows that M^{52} is absent from the amino acid sequence encoded by *bfrA*. The absence of M^{52} from the sequence of the *bfrA* product may render this protein incapable of binding heme, which led us to hypothesize that the *bfrA* gene encodes a bacterial ferritin (Ftn), not a bacterioferritin (Bfr).[22] The implication of this notion is that iron storage and management in the cytosol of *P. aeruginosa* are conducted by a bacterial ferritin (Ftn) and a bacterioferritin (Bfr), instead of a single bacterioferritin composed of two distinct subunits.

Available genetic information supports the idea of two ferritin-like molecules functioning independently in *P. aeruginosa*. In *Escherichia coli*, *P. aeruginosa*, and other organisms, the *bfrB* gene is next to a *bfd* gene, which encodes a bacterioferritin-associated ferredoxin.[36−39] In *P. aeruginosa*, iron starvation causes negative regulation of the *bfrB* gene[40] and strong positive regulation of the *bfd* gene.[41] In vitro, the efficient mobilization of iron from *Pa* BfrB requires the presence of apo *Pa* Bfd and delivery of electrons from *Pa* Fpr, which suggests that apo *Pa* Bfd acts as a regulator in the release of iron from *Pa* BfrB.[22] In *P. aeruginosa*, the *bfrA* gene is adjacent to a *katA* gene, which encodes a catalase active in all growth phases. A *bfrA* mutant of *P. aeruginosa* was found to express only 50% of the catalase activity of wild-type cells, while in contrast, a *bfrB* mutant did not have any effect on the catalase activity of the cell.[9] These observations taken together support the notion that the products of the *bfrA* and *bfrB* genes assemble into independent ferritin-like molecules that play different or redundant but independent roles in iron management.

To challenge the idea that iron metabolism in *P. aeruginosa* is aided by one bacterial ferritin and one bacterioferritin, rather than by a unique heterogeneous bacterioferritin, we have undertaken the biochemical and structural characterization of the proteins encoded by the *bfrA* and *bfrB* genes. In previous reports,

we showed that the product of the *bfrB* gene (*Pa* BfrB) is a genuine bacterioferritin assembled from 24 identical subunits and 12 heme molecules that harbors a symmetrical ferroxidase center typical of Bfr.[22,24] Herein, we report that the product of the *bfrA* gene is a protein assembled from 24 identical subunits that cannot bind heme. Its ferroxidase center is reminiscent of those typical of bacterial ferritins (Ftn) and is clearly distinct from the ferroxidase center of bacterioferritins. Hence, the structure of the so-called bacterioferritin A (BfrA) in *P. aeruginosa* reveals that this protein is a bacterial ferritin, and we propose that it should be termed *Pa* FtnA. We also found that the release of iron from *Pa* BfrB and *Pa* FtnA has different requirements. Whereas the release of iron from *Pa* BfrB requires the presence of a regulator (*Pa* Bfd) in addition to electrons supplied by a reductase,[22] the release of iron from *Pa* FtnA requires only the delivery of electrons from a reductase. These structural and functional properties, together with the available genetic information, strongly support the presence of two ferritin-like molecules in *P. aeruginosa*, a bacterial ferritin (*Pa* FtnA) and a bacterioferritin (*Pa* BfrB).

MATERIALS AND METHODS

Cloning of *P. aeruginosa bfrA*. The gene encoding *Pa* FtnA (PA4235) was synthesized, subcloned into a pET11a vector, and sequenced (GeneScript Corp., Pisctaway, NJ). The gene was engineered with silent mutations introducing codons favored by *E. coli*[42] and with *Nde*I and *Bam*HI restriction sites at the 5′ and 3′ ends, respectively, for subcloning. The pET11a/*bfrA* construct was transformed into *E. coli* BL21DE3 Gold cells (Stratagene) for protein expression.

Expression and Purification of *Pa* FtnA. A single colony of *E. coli* BL21(DE3) competent cells harboring the recombinant pET11-a/*bfrA* construct was cultured overnight at 37 °C in 50 mL of LB medium containing 100 μg/mL ampicillin. The 50 mL culture was used to inoculate 1 L of fresh LB medium (100 μg/mL ampicillin), which was shake-incubated (200 rpm) until the optical density at 600 nm (OD_{600}) was 0.6. The temperature was then lowered to 30 °C, and the culture was allowed to reach an OD_{600} of 0.8 before protein expression was induced by addition of IPTG (isopropyl 1-thio-D-galactopyranoside) to a final concentration of 1 mM. Cells were cultured for an additional 4 h at 30 °C before they were harvested by centrifugation and stored at −20 °C. Cell paste was resuspended (3 mL/g of cell paste) in 50 mM Tris-Base buffer (pH 7.6) containing 10 mM EDTA, 0.5 mM PMSF, protease inhibitor cocktail (Sigma Aldrich), and DNase (Sigma Aldrich) and lysed using a constant cell disruptor at 20 psi. Cell debris were pelleted by centrifugation at 4 °C and 19500 rpm for 45 min, and the supernatant was loaded onto a Q-Sepharose fast flow column [12 cm × 2.5 cm (inside diameter)] equilibrated with 20 mM Tris-Base and 1 mM EDTA (pH 7.6) at 4 °C. The column was washed with 3 bed volumes of the same buffer, and the protein was eluted with a linear gradient (from 0 to 600 mM) of NaCl. Fractions containing *Pa* FtnA were pooled and dialyzed against 4 L of 20 mM Tris-HCl and 1 mM EDTA (pH 7.6) at 4 °C, and the resultant solution was loaded onto a second Q-Sepharose fast flow column [12 cm × 2.5 cm (inside diameter)] and eluted as described above. Fractions containing *Pa* FtnA were pooled, and NaCl was added to a final concentration of ∼500 mM, to prevent protein precipitation during concentration by ultrafiltration (Ultracel 50K; Millipore). The concentrated solution (∼4 mL) was loaded onto a Sephacryl S-300 (GE Healthcare) size exclusion column [90 cm × 2.5 cm (inside diameter)] equilibrated with 50 mM Tris-HCl, 200 mM NaCl, and 1 mM EDTA (pH 7.6) at 4 °C. Fractions containing *Pa* FtnA were pooled, concentrated, and then loaded a second time onto the Sephacryl S-300 column, which typically resulted in homogeneous protein, as judged by sodium dodecyl sulfate−polyacrylamide gel electrophoresis (SDS−PAGE) (15%). In some preparations, it was necessary to pass the sample a third time through the Sephacryl S-300 column to obtain pure *Pa* FtnA.

The molecular mass of a *Pa* FtnA subunit was obtained by mass spectrometry using an ESI-MS Q-TOF mass spectrometer (Micromass Ltd., Manchester, U.K.). To this end, a 5 μM sample of *Pa* FtnA in 50 mM phosphate buffer (pH 7.4) was loaded onto a 0.5 mm inside diameter C4 reverse phase column (MC-5-C4, 300 Å pore size, Micro Tech). Elution was conducted by running an acetonitrile/isopropyl alcohol/water linear gradient of 4% acetonitrile/min at a rate of 10 μL/min from 20 to 60% acetonitrile (buffer A consisted of 99% water, 1% acetonitrile, and 0.08% formic acid; buffer B consisted of 80% acetonitrile, 10% isopropyl alcohol, 10% water, and 0.06% formic acid). The molecular mass of 24-mer *Pa* FtnA was estimated by FPLC (AKTA, Amersham Pharmacia Biotech) using a size exclusion column [Superdex 200 Prep, 60 cm × 16 cm (inside diameter) (GE Healthcare)], equilibrated with 50 mM sodium phosphate (pH 7.4), 150 mM NaCl, and 1 mM TCEP. The column was calibrated with a set of molecular mass standards (GE Healthcare) that included ferritin (440000 Da), aldolase (158000 Da), conalbumin (75000 Da), and carbonic anhydrase (29000 Da).

Loading *Pa* FtnA with Iron. Recombinant *Pa* FtnA, as isolated, contains a small amount of iron in its core, ∼10−15 iron ions per *Pa* FtnA 24-mer. To load *Pa* FtnA with iron, we prepared a solution of ferrous ammonium sulfate in a glovebox (Coy Laboratories), placed the solution in a container capped with a rubber septum, and removed the container from the anaerobic chamber. Concentrated HCl was added to the ferrous ammonium sulfate solution (50 μL/100 mL) through a septum using a Hamilton microsyringe needle; the resultant solution was added to a stirred solution of 0.2 μM *Pa* FtnA in 50 mM Tris (pH 7.4) at ambient temperature. Aliquots, which delivered approximately 10% of the total iron necessary to load each *Pa* FtnA molecule with ∼500 iron ions, were added approximately 15 min apart. The content of iron in the core was determined using a previously reported method.[22,43] A similar procedure[22] was used to load *Pa* BfrB with ∼550 iron ions.

Release of Iron from the Core of *Pa* FtnA and *Pa* BfrB. To study the release of iron stored in *Pa* FtnA and *Pa* BfrB, the proteins were mineralized with ∼500 iron ions and placed in an anaerobic glovebox.[22] Experiments to investigate the release of iron stored in *Pa* FtnA and *Pa* BfrB were conducted in the same anaerobic chamber, in a manner analogous to that reported previously for the release of iron from *Pa* BfrB.[22] Reactions were conducted in a 1.0 cm path length cuvette equipped with a magnetic stirring bar and containing a 3 mM solution of 2,2′-bipyridyl (bipy) in 20 mM potassium phosphate (pH 7.6). For the study of *Pa* FtnA, a few microliters from a stock solution of *Pa* FtnA and *Pa* Fpr was added to the cuvette to make the solution 0.25 μM in *Pa* FtnA and 10 μM in *Pa* Fpr. The reaction was initiated by addition of excess NADPH to a final concentration of 1.5 mM and the progress monitored by following the time-dependent changes in the intensity of the band at 523 nm upon

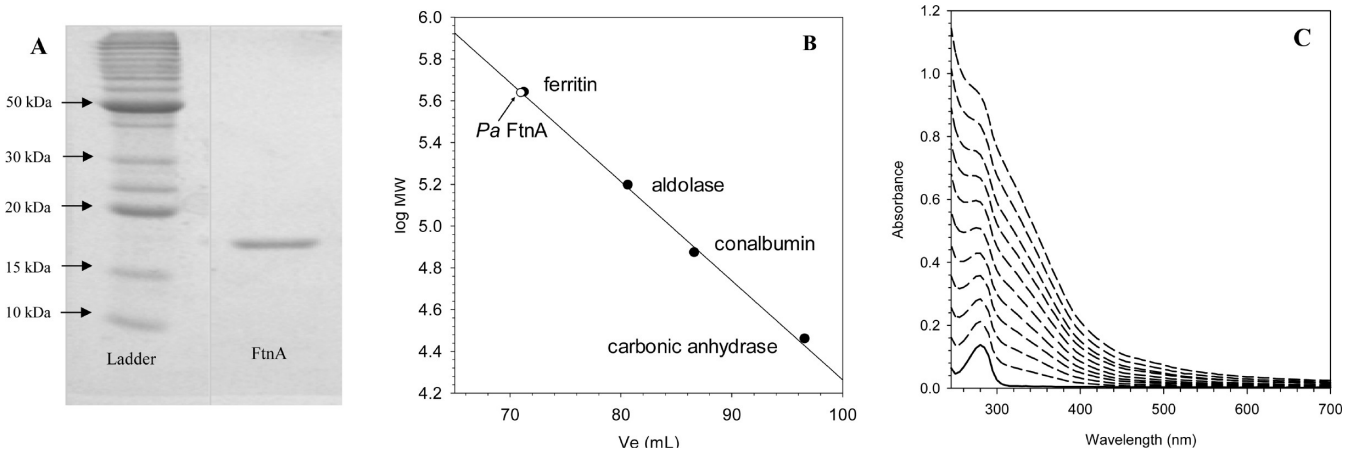

Figure 2. Characterization of recombinant *Pa* FtnA. (A) SDS−PAGE (15%) analysis of *Pa* FtnA purified to homogeneity. (B) Calibration curve obtained to estimate the molecular mass of 24-mer *Pa* FtnA constructed from the elution volume (V_e) of ferritin (440 kDa), aldolase (158 kDa), conalbumin (75 kDa), and carbonic anhydrase (29 kDa) loaded onto a Superdex 200 column equilibrated with 50 mM sodium phosphate (pH 7.4). (C) Family of spectra obtained during the reconstitution of core iron mineral in recombinant *Pa* FtnA [0.2 μM in 50 mM Tris (pH 7.4)]. The spectrum with the solid line, obtained prior to addition of Fe^{2+}, is compared with spectra obtained after subsequent addition of Fe^{2+} aliquots.

formation of the $[Fe(bipy)_3)]^{2+}$ complex. A similar procedure was used to study the release of iron from *Pa* BfrB, except that the cuvette also contained apo *Pa* Bfd, at concentrations described in the caption of Figure 7. Apo *Pa* Bfd was prepared in situ from holo *Pa* Bfd, using a procedure described previously.[22] In short, holo *Pa* Bfd was added to a stirred cuvette containing 3 mM bipy in 20 mM potassium phosphate (pH 7.6). Sodium dithionite (5 mM) was added to stoichiometrically reduce the Fe^{3+} in holo *Pa* Bfd to Fe^{2+}. Capturing of the ferrous ion by bipy was monitored by the time-dependent increase in the 523 nm absorbance, which was followed until it reached a plateau with intensity corresponding to the theoretical value calculated from the amount of holo *Pa* Bfd placed in the cuvette. At this point, the solution containing apo *Pa* Bfd was reconstituted with *Pa* Fpr and *Pa* BfrB and the iron mobilization reaction initiated by the addition of NADPH, as described above. Experiments involving apo *Pa* Bfd and *Pa* FtnA were conducted in an analogous manner. Please note that throughout these studies, Bfd stands for the C43S mutant of Bfd, which has previously been shown to behave like wild-type Bfd but can be expressed in higher yield and is more stable to storage and manipulation.[22]

Crystallization and Data Collection. *Pa* FtnA was concentrated to 8.0 mg/mL in 100 mM Tris buffer (pH 7.6) containing 200 mM NaCl and 1 mM EDTA for crystallization. Crystals were grown under aerobic conditions in Compact Jr. sitting-drop vapor diffusion plates (Emerald Biosystems) using 0.5 μL of protein and 0.5 μL of crystallization solution equilibrated against 100 μL of the latter. Crystals were obtained from three different conditions at 20 °C. (a) pH 6.0 crystals were obtained from Wizard2 #2 (Emerald Biosystems), 35% (v/v) 2-methyl-2,4-pentanediol, 100 mM MES (pH 6.0), and 200 mM Li_2SO_4. Crystals were transferred to a fresh drop of crystallization solution, which served as a cryoprotectant prior to the crystals being frozen in liquid nitrogen for data acquisition. (b) pH 7.5 crystals were obtained from Wizard 2 #5 (Emerald Biosystems), 20% (v/v) 1,4-butanediol, 100 mM HEPES (pH 7.5), and 200 mM NaCl. Crystals were transferred to a solution containing 80% crystallization solution and 20% glycerol for approximately 30 s before being frozen in liquid nitrogen for data collection. (c) pH 10.5 crystals were obtained from Wizard 2 #39 (Emerald Biosystems), 20% (w/v) PEG-8000, 100 mM CAPS (pH 10.5), and 200 mM NaCl. Crystals were transferred to a solution containing 80% crystallization solution and 20% PEG400 for approximately 30 s before being frozen in liquid nitrogen for data collection. To prepare samples with iron bound in the ferroxidase center, crystals obtained at each of the three pH values were soaked aerobically for 15 min in their respective crystallization solution containing 50 mM $FeCl_2$. Doubly soaked crystals were prepared by aerobically soaking crystals in 50 mM $FeCl_2$ for 15 min, followed by aerobically soaking them for 30 min in the same crystallization solution without $FeCl_2$. Single crystals at each of the pH values were transferred to the corresponding cryoprotection solution described above before being frozen in liquid nitrogen for data collection. X-ray diffraction data were collected at 100 K at the Advanced Photon Source (APS) IMCA-CAT, sector 17-BM, using an ADSC Quantum 210 CCD detector for apo pH 10.5 crystals at a λ of 1.0000 Å. Diffraction data for apo (pH 7.5) and Fe-soaked (pH 7.5) crystals were collected using a Mar 165 CCD detector at wavelengths (λ) of 1.0000 and 1.6531 Å. Data at 1.6531 Å were collected to obtain an anomalous signal from potentially bound Fe ions. Although the X-ray fluorescence K-edge emission peak of Fe has a maximum at approximately 1.74 Å, at 1.6314 Å prominent anomalous signals can be observed for Fe ions. Data for pH 6.0 and doubly soaked pH 7.5 *Pa* FtnA crystals were collected at APS sector 17-ID using a Pilatus 6M pixel array detector at a λ of 1.7401 Å, which was at the Fe absorption edge.

Structure Solution and Refinement. Intensities for as-isolated (pH 7.5) and Fe-soaked (pH 7.5) data sets were integrated and scaled using the HKL2000 package.[44] Intensities for all other data sets were integrated and scaled using XDS[45] and Scala,[46] respectively. The structure was initially determined via molecular replacement, using the as-isolated (pH 10.5) data set, with Molrep[47] using a single subunit of *Pa* BfrB (Protein Data Bank entry 3IS7) as the search model. The top solution yielding the highest correlation coefficient was obtained for a single monomer in the asymmetric unit in space group *F*432. The final *Pa* FtnA model obtained from the as-isolated pH 10.5 data was used

Table 1. Crystallographic Data for *Pa* FtnA Structures

	apo at pH 6.0	Fe-soaked at pH 6.0	doubly soaked at pH 6.0	apo at pH 7.5	Fe-soaked at pH 7.5	doubly soaked at pH 7.5	apo at pH 10.5
			Data Collection				
unit cell parameter	a = 171.34	a = 170.73	a = 171.16	a = 172.59	a = 172.52	a = 173.27	a = 173.12
space group	$F432$	$F432$	$F432$	$F432$	$F432$	$F432$	$F432$
resolution[a] (Å)	98.92−1.95 (2.06−1.95)	98.57−1.65 (1.74−1.65)	98.82−2.10 (2.21−2.10)	30.0−1.55 (1.61−1.55)	30.0−1.85 (1.92−1.85)	100.04−1.80 (1.90−1.80)	29.25−1.70 (1.79−1.70)
wavelength (Å)	1.7401	1.7401	1.7401	1.0000/1.6531	1.0000/1.6531	1.7401	1.0000
no. of observed reflections	595243	745089	486834	472881	204183	687618	1026694
no. of unique reflections	16285	25503	13093	32338	19371	21231	24998
$\langle I/\sigma(I)\rangle$[a]	30.2 (4.9)	20.8 (2.0)	33.0 (5.9)	42.9 (2.7)	33.4 (2.2)	23.3 (2.6)	27.6 (5.2)
completeness[a] (%)	100.0 (100.0)	97.3 (81.2)	100.0 (100.0)	99.4 (99.8)	99.9 (100)	100.0 (100.0)	100 (100)
multiplicity[a]	36.6 (34.5)	29.2 (4.0)	37.2 (37.9)	14.6 (14.7)	10.5 (10.3)	32.4 (16.2)	41.1 (36.6)
R_{merge}[a,b]	9.0 (84.9)	12.2 (58.8)	8.6 (76.5)	5.8 (72.4)	6.4 (80.5)	10.2 (88.4)	15.0 (87.0)
R_{pim} (%)[a,c]	1.5 (14.6)	2.1 (29.6)	1.5 (12.7)	not available	not available	1.8 (22.7)	2.4 (14.5)
			Refinement				
resolution (Å)	98.92−1.95	60.36−1.65	51.61−2.10	24.17−1.55	26.00−1.85	52.24−1.80	28.85−1.70
no. of reflections (working/test)	15463/819	24198/1293	12451/641	30356/1615	18364/990	20133/1091	23718/1274
R_{factor}/R_{free} (%)[d]	18.9/23.2	15.5/18.3	19.4/25.1	18.0/20.6	17.9/22.8	17.5/20.3	15.3/17.6
no. of atoms (protein/Fe/Na/SO_4/water)	1258/0/ 1/8/96	1294/3/ 1/3/178	1269/4/ 1/3/64	1299/0/ 3/0/164	1295/5/ 1/0/134	1284/3/ 1/0/185	1279/0/ 3/0/179
			Model Quality				
root-mean-square deviation							
bond lengths (Å)	0.019	0.014	0.016	0.020	0.017	0.014	0.016
bond angles (deg)	1.482	1.416	1.460	1.221	1.420	1.294	1.373
average B factor (Å^2)							
all atoms	34.2	16.9	38.3	17.6	25.4	25.0	14.7
protein	33.5	15.2	37.9	16.1	24.4	23.6	13.0
water	42.2	28.7	43.9	17.6	24.3	34.3	25.0
iron/sodium	−/31.2	27.1/11.9	62.0/46.0	−/16.1	40.1/38.3	47.7/44.8	−/18.0
sulfate	43.9	24.2	44.0	−	−	−	−
coordinate error based on maximum likelihood (Å)	0.22	0.14	0.20	0.18	0.18	0.23	0.15
Ramachandran plot							
favored (%)	98.7	99.4	99.3	98.8	98.7	98.7	99.4
additionally allowed (%)	1.3	0.6	0.7	1.2	1.1	1.3	0.6

[a] Values in parentheses are for the highest-resolution shell. [b] $R_{merge} = \Sigma_{hkl}\Sigma_i|I_i(hkl) - \langle I(hkl)\rangle|/\Sigma_{hkl}\Sigma_i I_i(hkl)$, where $I_i(hkl)$ is the intensity measured for the ith reflection and $\langle I(hkl)\rangle$ is the average intensity of all reflections with indices hkl. [c] R_{pim} is the precision-indicating (multiplicity-weighted) R_{merge}.[55] [d] $R_{factor} = \Sigma_{hkl}||F_{obs}(hkl)| - |F_{calc}(hkl)||/\Sigma_{hkl}|F_{obs}(hkl)|$. R_{free} is calculated in an identical manner using 5% of randomly selected reflections that were not included in the refinement.

for subsequent molecular replacement searches against all other data sets. Structure refinement and manual model building were performed with Phenix[48] and Coot,[49] respectively. Structure validation was performed using Molprobity,[50] and figures were prepared with CCP4mg.[51]

Following initial refinement, certain iron atoms, for a particular structure, contained negative electron density ($F_o - F_c$) and B factors that were approximately twice that of the Fe_A site. The anomalous difference maps were examined, and peak heights and B factors of the Fe atoms were compared for each particular structure. Occupancy factors were manually adjusted to values ranging from ∼0.3 to ∼0.5 (see below), the structures refined, and the electron density maps and B factors analyzed. Occupancies for the Fe ions were set as follows. (i) For Fe-soaked at pH 6.0, the anomalous peak heights were similar for all iron atoms and were therefore refined with full occupancy factors. (ii) For the double soak at pH 6.0, anomalous density peak heights for the Fe sites were 43.2σ (Fe_A), 19.6σ (Fe_B), 22.7σ (Fe_C), and 20.7σ (Fe_{His130}). Assuming an occupancy factor of 1.0 for Fe_A, all other Fe atoms were refined with occupancy factors of 0.5. (iii) For the Fe soak at pH 7.5, anomalous peak heights were 20.6σ (Fe_A), 21.1σ (Fe_B), and approximately 8σ (Fe_C, Fe_D, and Fe_E); thus, sites Fe_C−Fe_E were refined with occupancy factors of 0.5. (iv) For the double soak at pH 7.5, anomalous peak heights were 45.5σ (Fe_A), 42.1σ (Fe_B), and 20.4σ (Fe_C), so the latter was refined with an occupancy factor of 0.5. Automated refinement of the occupancies for partially occupied Fe ions along with the B factors in Phenix resulted in occupancy factors that were similar to those determined manually (approximately 0.5).

dx.doi.org/10.1021/bi2004119 |*Biochemistry* 2011, 50, 5236–5248

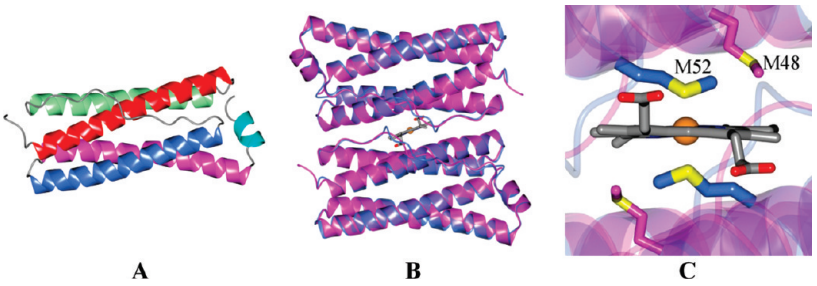

Figure 3. (A) Secondary structure of *Pa* FtnA showing helices A (red), B (green), C (blue), D (magenta), and E (cyan). (B) Superposition of a *Pa* BfrB noncrystallographic dimer (blue, Protein Data Bank entry 3IS7) and a Pa FtnA crystallographic dimer (magenta), viewed along the 2-fold axis. The heme from *Pa* BfrB is colored gray. (C) Close-up showing M^{52} of *Pa* BfrB binding heme (blue) and the relative position of the closest Met residue in *Pa* FtnA, M^{48}.

RESULTS

Overexpression, Purification, and Characterization of *Pa* FtnA. Recombinant FtnA expressed in *E. coli* BL21DE3 cells was purified to homogeneity, as determined by the presence of a single band (~18 kDa) in an SDS−PAGE gel (Figure 2A). The molecular mass of a subunit was determined by electrospray ionization mass spectrometry to be 17939 Da, a value in excellent agreement with that calculated from the amino acid sequence (17940 Da), including the initiator methionine. The elution volume (V_e) of *Pa* FtnA from a calibrated size exclusion column is nearly identical to the V_e of a (eukaryotic) ferritin standard purchased from GE Healthcare (Figure 2B). The molecular mass of FtnA, estimated from its V_e (436.3 kDa), is in good agreement with the value of 430.6 kDa calculated from the amino acid sequence, thus demonstrating the structural integrity of the 24-mer FtnA assembly.

Preparation of Iron-Loaded *Pa* FtnA. Protein containing ~520 ± 20 iron atoms per *Pa* FtnA molecule was prepared by titrating an anaerobic solution of Fe^{2+} into a solution of *Pa* FtnA in air. As described previously for the mineralization of *Pa* BfrB,[22] aliquots of Fe^{2+}, each containing ~10% of the total iron, were added approximately 15 min apart to allow for uptake and mineralization. The corresponding spectra (Figure 2C) show a gradual increase in the absorption at ~280 nm with good preservation of baseline, which indicates that the capture of Fe^{2+}, and its subsequent oxidation and mineralization, are efficiently achieved by *Pa* FtnA.

X-ray Crystallography. Crystals of *Pa* FtnA were obtained at pH 6.0, 7.5, and 10.5. Diffraction data were collected from crystals grown at each of the pH values from the protein as isolated (as-isolated *Pa* FtnA), after crystals of as-isolated *Pa* FtnA had been soaked in a solution of $FeCl_2$ dissolved in crystallization solution (Fe-soaked *Pa* FtnA) and after crystals of Fe-soaked *Pa* FtnA had been soaked in crystallization solution in the absence of $FeCl_2$ (doubly soaked *Pa* FtnA). The relevant crystallographic data are summarized in Table 1. The overall structures obtained from crystals at pH 6.0, 7.5, and 10.5 are nearly identical; small but important and informative differences exist in the ferroxidase center in the Fe-soaked and doubly soaked structures. These differences will be discussed below, after we present relevant information obtained from the overall fold.

The *Pa* FtnA structure conforms to the fold typical of ferritin-like molecules and consists of an assembly of 24 identical subunits forming a nearly spherical shape with 4,3,2 point symmetry. The fold of each *Pa* FtnA subunit consists of a four-α-helix bundle (helices A−D) and a fifth, short α-helix (E) that is nearly perpendicular to the four-helix bundle (Figure 3A). Figure 3B shows a superposition of a *Pa* FtnA dimer (magenta) with its equivalent in *Pa* BfrB (blue) viewed along the 2-fold axis of symmetry, which passes through the heme iron. Evidently, the folds are nearly identical, except for the fact that *Pa* FtnA does not contain heme. In *Pa* BfrB and in all bacterioferritins of known structure, the axial ligands coordinating a heme molecule are two M^{52} side chains, one from each subunit in a dimer. Each M^{52} can axially coordinate the heme iron because the location of each at the center of the B helix places them relatively close to one another and in an ideal geometry (collinear with the C_2 axis) to bind each of the two axial sites of a heme molecule (blue in Figure 3C). In contrast, and because of the 2-fold symmetry of a subunit dimer, residues located on either side of the center of the B helix become increasingly separated from one another and therefore incapable of acting as heme axial ligands. In the amino acid sequence of *Pa* FtnA, position 52 (center of helix B) is occupied by Thr. The Met residue closest to the center of the B helix is M^{48} (magenta in Figure 3C); its position, relatively far from the C_2 axis, precludes the M^{48} side chains in a dimer from functioning as axial ligands to the heme iron. These structural observations, which are consistent with the absence of heme in *Pa* FtnA, clearly demonstrate that it did not evolve to bind heme, a property that relates it to bacterial ferritins and clearly separates it from bacterioferritins.

The Ferroxidase Center in As-Isolated *Pa* FtnA Is Empty. As isolated, recombinant *Pa* FtnA (pH 6.0, 7.5, or 10.5) does not have iron in the ferroxidase center. Prominent difference electron density was observed in the ferroxidase center of the pH 10.5 structure, but structural refinement that included Fe or water molecules in the model resulted in residual negative or positive difference density, respectively. A model that includes sodium ions, on the other hand, refined to an *R* factor of 15.3 and satisfied coordination geometry and bond lengths to respective ligands. Hence, the prominent difference electron density in the ferroxidase center of as-isolated *Pa* FtnA (pH 10.5) most likely corresponds to two sodium ions (green, Figure 4). E^{18} and H^{54} serve as capping ligands to Na_1, E^{51} as a bridging ligand and E^{93} as a capping ligand to Na_2 (green in Figure 4); the side chain of H^{130} is rotated away from Na_2 in a conformation very similar to the "gate open" conformation of H^{130} in the ferroxidase empty structure of *Pa* BfrB.[24] The ferroxidase center in the pH 7.5 structure (magenta in Figure 4) also harbors two sodium ions in very similar positions. In addition, no anomalous difference electron density was observed in the ferroxidase center using diffraction data collected near the Fe absorption edge. H^{130} in

dx.doi.org/10.1021/bi2004119 |*Biochemistry* 2011, 50, 5236–5248

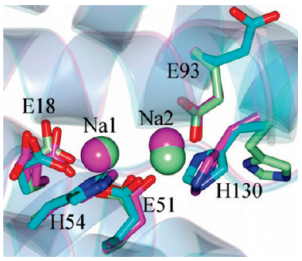

Figure 4. Superposition of as-isolated *Pa* FtnA structures obtained from crystals grown at pH 6.0 (cyan), pH 7.5 (magenta), and pH 10.5 (green) showing the ferroxidase center. Sodium ions are drawn as spheres.

this structure is rotated toward Na_2 but does not bind it, whereas the side chain of E^{18} is in two conformations, one that coordinates Na_1 and the other rotated away from it. In the pH 6.0 structure (cyan in Figure 4), the ferroxidase center is devoid of metal ions, and the side chains of E^{18} and E^{93} are rotated away from the positions occupied by Na_1 and Na_2 in the pH 7.5 and 10.5 structures. These conformational changes, which in the crystal structures are likely "snapshots" of predominant populations, suggest a dynamic ferroxidase center tuned to respond to changes in coordination state and local pH.

Iron-Loaded Ferroxidase Center of *Pa* FtnA. Soaking crystals of as-isolated *Pa* FtnA in crystallization solution containing 50 mM $FeCl_2$ (pH 6.0 and 7.5), followed by collection of X-ray diffraction data, resulted in structures with iron at the ferroxidase center; soaking crystals grown at pH 10.5 resulted in precipitation of the $FeCl_2$. Figure 5A shows a close-up of the ferroxidase center in the *Pa* FtnA structure (pH 6.0) where Fe_A and Fe_B (orange) are coordinated by capping ligands E^{18} and H^{54}, and E^{93} and H^{130}, respectively, and bridged by E^{51} and by a water molecule (red). The presence of iron is corroborated in the prominent difference electron density ($F_o - F_c$) and by the strong anomalous signal (blue mesh) from data acquired at 1.7401 Å. An identical view depicting $2F_o - F_c$ electron density maps of ferroxidase iron ligands is shown in Figure S2 of the Supporting Information. The architecture of the *Pa* FtnA ferroxidase center, with only one bridging ligand provided by the protein, is reminiscent of bacterial and eukaryotic ferritins and clearly distinct from the ferroxidase center of bacterioferritins (see Figure 1). The view of Figure 5A also shows the presence of a third iron ion (Fe_C), which is coordinated by H^{46}, E^{50}, and four water molecules. This iron ion is similar to site C iron, first observed in the iron-soaked structure of *E. coli* FtnA[29] and subsequently in the Ftn proteins of *Archeoglobus fulgidis*[31] and *Py. furiosus*.[32] An interesting distinction is the fact that in *Pa* FtnA H^{130} acts exclusively as a capping ligand to Fe_B, whereas in the ferroxidase center of *E. coli*, *A. fulgidis*, and *Py. furiosus* Ftn, the equivalent capping ligand, E^{130}, also coordinates Fe_C. Hence, the unique presence of His at position 130 not only constitutes a new Ftn ferroxidase center architecture but also represents a unique binding mode of Fe at site C. This structure (pH 6.0) was refined with full-occupancy factors for all three types of iron (see Materials and Methods).

Superposition of the full (cyan) and apo (purple) ferroxidase centers (pH 6.0) illustrates the conformational rearrangement in the side chains of E^{18} and E^{93} and the minimal changes in the side chains of E^{51}, H^{54}, and H^{130} upon binding of iron (Figure S3 of the Supporting Information). Similar observations are made upon comparison of the ferroxidase full and empty structures

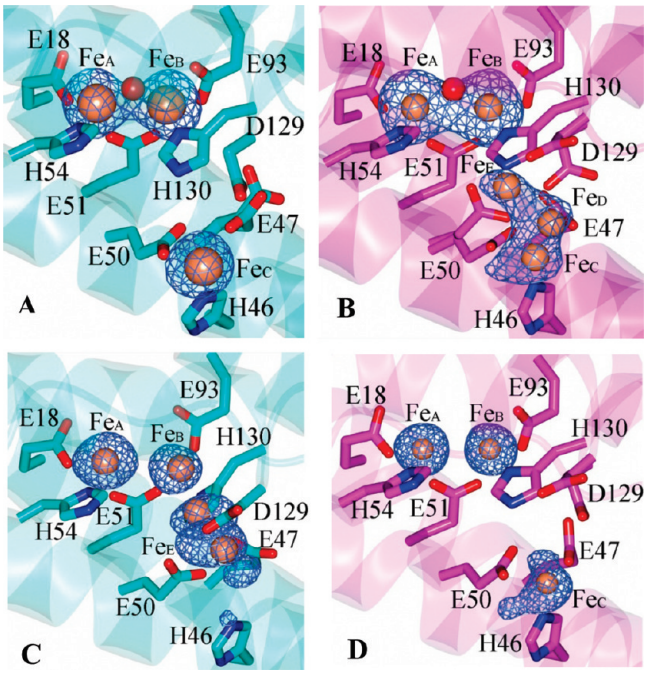

Figure 5. Phased anomalous difference maps (blue mesh) of the ferroxidase center of *Pa* FtnA Fe soaked and doubly soaked, contoured at 5σ: (A) pH 6.0 Fe soak (λ = 1.7401 Å), (B) pH 7.5 Fe soak (λ = 1.6531 Å), (C) pH 6.0 doubly soaked (λ = 1.7401 Å), and (D) pH 7.5 doubly soaked (λ = 1.7401 Å). Identical views depicting $2F_o - F_c$ electron density maps of the ferroxidase iron ligands are shown in Figure S2 of the Supporting Information.

obtained at pH 7.5, where the most significant change is the collapse of the two alternative conformations of the E^{18} side chain into one, iron-bound conformation.

A similar view of the ferroxidase center in the iron-soaked pH 7.5 structure (Figure 5B) shows the presence of three iron ions, Fe_C—Fe_E, in addition to Fe_A and Fe_B. These additional iron ions exhibit anomalous peak intensities that are approximately one-half of the peak intensities exhibited by Fe_A and Fe_B. Hence, as described in Materials and Methods, Fe_C—Fe_E were refined assuming occupancies of 0.5. An identical view depicting $2F_o - F_c$ electron density maps of the ferroxidase ligands is shown in Figure S2B of the Supporting Information. It is noteworthy that the side chains of E^{50} and D^{129} exhibit two conformations, which allow these residues to bind two iron ions; i.e., E^{50} binds Fe_C and Fe_D, and D^{129} binds Fe_D and Fe_E. These observations suggest that the structure is a composite of several populations that allow visualization of the process of migration of iron from the ferroxidase center to the core mineral; the location of Fe_D and Fe_E provides a good idea of the path followed by iron, and the multiple conformations of the amino acid side chains involved underscore the role played by side chain coordination and motion in propelling iron along the internal wall of the ferritin molecule. The distance between ferroxidase iron ions (Fe_A and Fe_B) in the pH 6.0 and 7.5 structures is 3.4 Å, which is typical of di-Fe^{3+} sites in diiron proteins such as ribonucleotide reductase and methane monooxygenase.[52] In both Fe-soaked structures, Fe_A and Fe_B are bridged by well-defined and spherically symmetric electron density, which was refined as a water molecule but could also be a μ-oxo or μ-hydroxo ligand bridging the Fe^{3+} ions. In both structures, Fe_C is 10.2 Å from the nearest

ferroxidase iron (Fe_B) and 11.2 Å from Fe_A; these distances are larger than those separating Fe_C from Fe_B and Fe_A (~6.3−7.4 Å) in the structure of archaeal and bacterial ferritins of known structure. In the pH 7.5 FtnA structure, Fe_D is 8.1 Å from Fe_B and 9.8 Å from Fe_A, whereas Fe_E, which is the iron ion closest to the ferroxidase center, is 7.8 Å from Fe_B and 8.6 Å from Fe_A. The distance between Fe_D and Fe_E is 3.4 Å, and the distance between Fe_C and Fe_D is 2.6 Å.

Attempts To Empty the Ferroxidase Center *in Crystallo*. In a previous report, we showed that the ferroxidase center of *Pa* BfrB is readily empty, in solution, and upon incubation of an iron-soaked crystal in crystallization solution.[24] These structural observations and kinetic studies of iron uptake revealed that the ferroxidase center of *Pa* BfrB is likely the dominant port of entry of Fe^{2+} into the cavity of *Pa* BfrB.[24] In an attempt to learn something about the path followed by iron on its way to the interior of *Pa* FtnA, we conducted experiments in which crystals soaked in iron solution were subsequently soaked in crystallization solution that did not contain iron, prior to freezing and data acquisition. Observations made with crystals grown at pH 6.0 are summarized in Figure 5C. Two features of Fe_B in the doubly soaked structure are noteworthy. (i) The intensity of its anomalous peak is approximately one-half of that of Fe_A, and (ii) its position reveals that it is displaced ~1 Å toward the interior cavity relative to Fe_A in the iron-soaked structure. In addition, a "trail" of anomalous electron density can be traced from Fe_B passing through the volume occupied by the imidazole ring of H^{130} and ending at a position similar to that occupied by Fe_E in the pH 7.5 structure; Fe_C is not observed. It is important to note that although difference electron density for the ferroxidase iron ligands is well-defined, that corresponding to the imidazole ring in H^{130} can be best described by at least two conformations related by rotation about the $C^{\beta}-C^{\gamma}$ bond. The electron density ($2F_o - F_c$) for the imidazole ring of H^{130} displayed a nearly spherical shape (Figure S2C of the Supporting Information), making it difficult to discern its orientation. In addition, positive difference density ($F_o - F_c$) was observed at the imidazole ring following refinement. The most striking observation, however, is anomalous electron density from iron sharing the same volume in space with electron density from the imidazole ring of H^{130}. We interpret these observations to indicate that the data represent a weighted average of several local structures differing in the position of iron as it trails from Fe_B toward Fe_E, across the position occupied by the side chain of H^{130} when coordinated to Fe_B. For iron to slide through the position occupied by the H^{130} side chain, the latter has to move out to an alternative conformation. The absence of electron density corresponding to a unique alternative conformation, however, suggests that the side chain populates several conformations rather than a predominant "gate open" conformation. Taken together, the observations strongly suggest that the local structure captured in this snapshot is a composite of several populations that allow visualization of a path followed by Fe_B as it moves toward site C. The results also underscore the fact that iron translocation is made possible by the conformational flexibility of the H^{130} side chain, which may function in a dual role of iron ligand at the ferroxidase center and iron gate to allow entry of ferroxidase iron into the interior cavity, which has been shown for the equivalent H^{130} in the ferroxidase center of *Pa* BfrB.[24]

Results from similar double-soak experiments conducted with crystals grown at pH 7.5 are summarized in Figure 5D. In this structure, ferroxidase center ions Fe_A and Fe_B exhibit very similar anomalous peak intensities that are nearly twice as intense as that corresponding to Fe_C. The most important difference when compared to the Fe soak structure at pH 7.5 (Figure 5B) is the absence of Fe_D and Fe_E, which lends support to the idea that these positions correspond to transient iron moving toward the interior cavity, where the last observable stop is Fe_C, before iron is incorporated into the growing mineral. The two conformations observed for D^{129} help preserve the idea that the conformational flexibility of coordinating side chains on the interior surface plays important roles in the internalization of iron. It is also interesting to contrast the relative populations of Fe_A and Fe_B in the Fe-soaked and doubly soaked structures obtained at pH 6.0 and 7.5. In the Fe-soaked structures at both pH values, the anomalous peak intensities of the Fe_A and Fe_B ions are nearly identical, which we interpret to indicate nearly full and equal population of the Fe_A and Fe_B sites. The double-soak experiments, on the other hand, reveal interesting differences. In the pH 7.5 structure, ferroxidase sites Fe_A and Fe_B appear to remain nearly fully populated, which suggests that at this pH, *in crystallo*, the ferroxidase center of *Pa* FtnA is relatively stable. In comparison, the pH 6.0 structure shows that Fe_B has moved toward the interior cavity and its intensity is approximately one-half of that of Fe_A, thus suggesting that at pH 6.0, *in crystallo*, ferroxidase iron moves toward the interior, where it is incorporated into the growing mineral. It is important to stress, however, that these crystallographic observations are not sufficient to allow speculation about a mechanism for incorporation of iron into *Pa* FtnA; elucidation of such a mechanism will require detailed kinetic studies in solution.

Three- and Four-Fold Pores. Unlike the three-fold pores of *Ec* FtnA, which are plugged by hydrophobic residues (M^{109} and F^{117}),[29] the three-fold pores of *Pa* FtnA are lined with side chains of alternating charge. The outermost layer is formed by the side chains of E^{108} and D^{117}, which interact electrostatically with the innermost layer composed of R^{116} and K^{120}. In the pH 6.0 structure, a sulfate ion is observed between the two layers of the pore (Figure 6A and Figure S4 of the Supporting Information), where it is stabilized by electrostatic interactions with the positively charged residues in the inner layer (Figure 6A); the source of sulfate is the crystallization solution, which contains 200 mM Li_2SO_4. By comparison, in the pH 7.5 and 10.5 structures, the three-fold pores have nearly identical structure, except that water molecules occupy the majority of the volume.

Four-fold pores in *Pa* FtnA assemble at the junction of four subunits (Figure 6C). Viewed from the exterior, the pore perimeter is outlined by the last turn of helix D and by the loop connecting helix D to helix E. The pore walls are formed by a section of helix E, from which stem ligands (N^{148} and Q^{151}) that coordinate a Na^+ ion observed in the four-fold pores of all the structures reported herein, including the Fe-soaked and doubly soaked structures. The possibility that the metal ion in the four-fold pore is iron was eliminated by the absence of anomalous electron density in data sets collected at wavelengths of 1.6314 and 1.7401 Å. In addition, residual difference density, negative or positive, is observed when iron or a water molecule is modeled at these sites, respectively. The presence of Na^+ in the four-fold pores likely stems from the composition of the purification and storage buffers (see Materials and Methods). The ligands coordinating the Na^+ ions in the four-fold pores of *Pa* FtnA are identical to those coordinating K^+ observed in the four-fold pores of *Pa* BfrB,[24] and Fe^{2+} or Ba^{2+} in bacterioferritin from *Azotobacter vinelandii*.[26,53] In comparison, the four-fold pores of

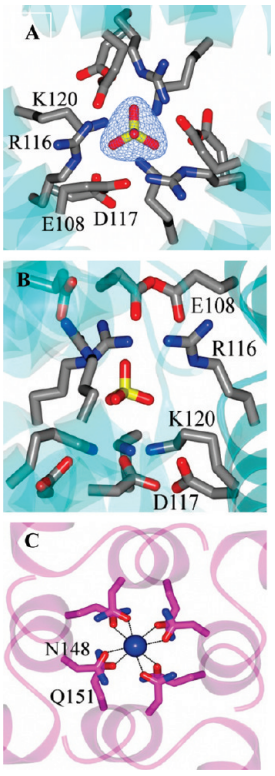

Figure 6. (A) View along a three-fold pore in *Pa* FtnA (pH 6.0) showing a sulfate ion (yellow) positioned between an inner layer of positively charged residues R^{116} and K^{120}; negatively charged residues E^{108} and D^{117} occupy the outer layer. The $2F_o - F_c$ electron density map for the sulfate ion, contoured at 1σ, is shown as blue mesh. (B) View normal to the three-fold pore axis showing the layers of positively and negatively charged residues. (C) View of a four-fold pore in *Pa* FtnA (pH 6.0) showing the residues that coordinate a sodium ion (blue sphere).

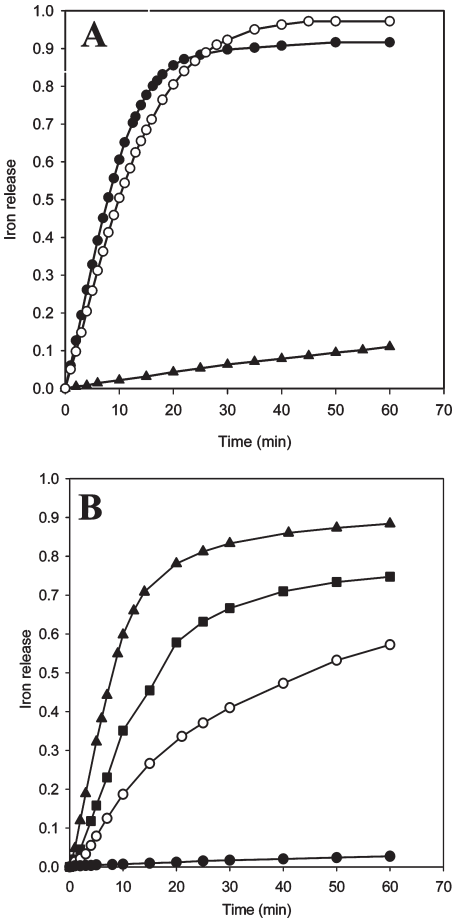

Figure 7. Release of iron from *Pa* FtnA and *Pa* BfB has different regulatory needs. (A) Time-dependent increase in normalized ΔA_{523} upon addition of excess NADPH (final concentration of 1.5 mM) to 20 mM phosphate buffer (pH 7.6) containing: (▲) *Pa* FtnA (0.25 μM), (○) *Pa* FtnA (0.25 μM) and *Pa* Fpr (10 μM), and (●) *Pa* FtnA (0.25 μM), *Pa* Fpr (10 μM), and apo *Pa* Bfd (10 μM); the apo *Pa* Bfd:FtnA ratio was 40. (B) Time-dependent increase in normalized ΔA_{523} upon addition of excess NADPH (final concentration of 1.5 mM) to a solution containing *Pa* BfrB (0.37 μM), *Pa* Fpr (15 μM), and apo *Pa* Bfd with Bfd:BfrB molar ratios of 0 (●), 5 (○), 15 (■), and 40 (▲).

Ec FtnA are lined by hydrophilic and hydrophobic residues, with four E^{149} side chains forming the outermost layer, four F^{153} side chains constituting a middle layer, and four K^{156} side chains the innermost layer.[29] The hydrophilic nature of the residues in the four-fold pores of bacterioferritins from *P. aeruginosa* and *Az. vinelandii* is consistent with the crystallographic observation of metal ions bound to the four-fold pores of these structures, observations that have led to the suggestion that Fe^{2+} may move in or out of the Bfr cavity via these conduits.[24,26,53] It is therefore interesting that the structures of the four-fold pores in FtnA, including their avidity for metal ions, are nearly identical to those of the structures of bacterioferritins from *P. aeruginosa* and *Az. vinelandii*, because it suggests that Fe^{2+} may also move in or out of the *Pa* FtnA structure via the four-fold pores in its structure.

Release of Iron from *Pa* FtnA. Experiments directed at studying the mobilization of core iron from *Pa* FtnA were conducted in an anaerobic glovebox using methods described previously for the study of release of iron from the core of *Pa* BfrB.[22] In brief, the release of iron was initiated by addition of NADPH to a cuvette containing a solution of bipy and *Pa* FtnA mineralized with ~500 iron ions. The process was monitored by following ΔA_{523}, the time-dependent formation of $[Fe(bipy)_3]^{2+}$. The triangles in Figure 7A track ΔA_{523} normalized to the total change in absorbance expected upon removal of all the iron ions from the cavity of the ferritin, following addition of NADPH to a solution containing 0.25 μM *Pa* FtnA. The black circles track normalized ΔA_{523} upon addition of NADPH to a mixture of *Pa* FtnA (0.25 μM) and *Pa* Fpr (10 μM). Evidently, *Pa* Fpr is capable of mediating electrons from NADPH to the core of *Pa* FtnA to reduce Fe^{3+} and allow the efficient release of Fe^{2+} from *Pa* FtnA. A pseudo-first-order rate constant of iron release (0.092 ± 0.003 min^{-1}) was estimated by fitting the curve to an exponential function. Results from a similar experiment conducted with a solution containing 0.25 μM *Pa* FtnA, 10 μM *Pa* Fpr, and 10 μM apo *Pa* Bfd (apo *Pa* Bfd:*Pa* BfrB ratio of 40) are depicted by the empty circles in Figure 7A. This experiment shows a rate of iron release (pseudo-first-order rate constant of 0.078 ± 0.004 min^{-1}) similar to that obtained in the absence of apo *Pa* Bfd, thus demonstrating that release of iron from *Pa* FtnA is independent of the presence of apo *Pa* Bfd. This behavior is in striking contrast with that previously observed with *Pa* BfrB, which requires not only *Pa* Fpr to mediate electrons from NADPH but also the binding of apo *Pa*-Bfd to release iron.[22] To facilitate comparison, in Figure 7B we show results from similar experiments conducted with *Pa* BfrB mineralized with

~550 iron ions. In the absence of apo *Pa* Bfd, addition of NADPH to a solution containing *Pa* BfrB (0.37 μM) and *Pa* Fpr (15 μM) is followed by a slow release of Fe^{2+} (●). The rate of Fe^{2+} release, however, can be accelerated in an apo *Pa* Bfd-dependent manner. This is evident from the traces delineated by empty circles, squares, and triangles, which correspond to experiments in which the apo *Pa* Bfd:*Pa* BfrB ratio was 5, 15, and 40, respectively, which results in corresponding pseudo-first-order rate constants of 0.030 ± 0.001, 0.058 ± 0.008, and 0.101 ± 0.004 min^{-1}, respectively. Clearly, efficient release of iron stored in *Pa* FtnA requires only the input of electrons from *Pa* Fpr, whereas release of iron from *Pa* BfrB requires the presence of apo *Pa* Bfd, in addition to *Pa* Fpr. These observations indicate different regulatory mechanisms for the process of release of iron from *Pa* BfrB and from *Pa* FtnA and strongly support the idea that these two distinct types of ferritin-like molecules have specific and likely independent roles in iron management in the cytosol of *P. aeruginosa*.

■ DISCUSSION

Bacteria have two types of 24-mer ferritin-like molecules, Ftn and Bfr. Although these proteins may play more than one role in the cell, so far it is clear that they participate in iron storage and delivery and in detoxification of the pro-oxidant Fe(II), thereby acting as dynamic regulators of cytosolic iron concentrations. In bacteria harboring both Bfr and Ftn, it is not known which plays a dominant role in iron storage, but it is likely that the significance of their respective participation in iron homeostasis is largely dictated by the environment surrounding the cell. *P. aeruginosa* was thought to harbor only one ferritin-like molecule assembled from two different bacterioferritin subunits, α and β. The idea of a single, mixed chain bacterioferritin in *P. aeruginosa*, however, can be challenged in light of more recent studies showing that the *bfr*α and *bfr*β genes appear to be regulated differently[40,41] and expressed independently of one another.[9,40] In this report, we present structural and functional evidence supporting the notion that the products of the *bfr*α and *bfr*β genes are two distinct ferritins. The product of *bfr*α assembles into a 24-mer not capable of binding heme. The structure of its ferroxidase center is similar to that of the diiron center of bacterial and eukaryotic ferritin in that Fe_A and Fe_B are bridged by only one protein-provided ligand (E^{50}), which contrasts with the structure of the characteristically symmetric ferroxidase centers of Bfrs, where Fe_1 and Fe_2 are bridged by two glutamate ligands (Figure 1). These structural properties indicate that the product of the *bfr*α gene is not a bacterioferritin, but a bacterial ferritin, which we propose should be termed *Pa* FtnA. The ferroxidase center of *Pa* FtnA is fully functional and allows the protein to efficiently capture Fe^{2+}, oxidize it, and store Fe^{3+} in its core. Although its structure is similar to that seen in *Ec* FtnA, it is not identical because Fe_B in *Pa* FtnA is coordinated by E^{94} and H^{130}, whereas that of bacterial and archaeal ferritins of known structure binds Fe_B using two Glu ligands [E^{94} and E^{130} in *Ec* FtnA (see Figure 1)]. Hence, the chemical environment of Fe_B in *Pa* FtnA imparts its ferroxidase center with a previously unobserved structure.

The structures of *E. coli*, *Py. furiosus*, and *A. fulgidus* ferritins revealed the presence of a third iron ion near the ferroxidase center, which has been termed site C (Figure 1). The iron-soaked structure of *Pa* FtnA at pH 6.0 shows the presence of a third iron ion (Fe_C) in addition to ferroxidase iron. Fe_C in *Pa* FtnA, however, is not completely equivalent to site C in *E. coli* and archaeal ferritins because the latter is coordinated by E^{49}, E^{126}, and E^{129}, whereas Fe_C in *Pa* FtnA is coordinated by H^{46} and E^{50} (Figure 5A). Fe_C was also observed in the iron-soaked structure of *Pa* FtnA at pH 7.5 (Figure 5B), together with two additional iron ions, Fe_D and Fe_E. In both structures, the anomalous peak intensity defining these iron ions ($Fe_C - Fe_E$) is roughly one-half the anomalous peak intensity corresponding to feroxidase ions Fe_A and Fe_B, suggesting that these are transient sites in the process of translocation of iron from the ferroxidase center to the growing mineral in the interior of the ferritin. The multiple conformations of the side chains coordinating Fe_C and Fe_D add support to this idea because they suggest that iron is propelled along the path delineated by Fe_C, Fe_E, and Fe_D by conformational changes of coordinative side chains. This notion finds additional support in the observations made while attempting to empty the ferroxidase center *in crystallo* by soaking Fe-soaked crystals in crystallization solution at pH 6.0 (Figure 5C). Particularly revealing are the findings that Fe_B has moved away from its position in the ferroxidase center toward the interior cavity and that an iron ion appears to occupy the same volume in the structure as the side chain of H^{130}, because they suggest that internalization of Fe_B along this path requires temporary relocation of the H^{130} side chain.

Placed together, the observations suggest that internalization of an iron ion from the ferroxidase center is facilitated by a gating function of H^{130} in the ferroxidase center of *Pa* FtnA. The path followed by iron on its way to Fe_c may be roughly delineated by a combination of the snapshots provided in panels B and C of Figure 5. The conformational changes that gate iron entry are likely aided by proton transfer reactions that alter the ionization state of ferroxidase ligands and by electron transfer reactions that change the oxidation state of iron at the ferroxidase center. The distinct conformations of ferroxidase ligands in structures obtained at different pH values (Figure 4) underscore their propensity to respond to local pH changes and highlight a possible role for proton transfer reactions. The dynamic relocation of H^{130} that facilitates internalization of oxidized iron (Figure 5C and Figure S2C of the Supporting Information) suggests that the conformational state of key ferroxidase ligands is also dependent on the oxidation state of iron at the ferroxidase center. Clearly, confirmation of these ideas derived from structural considerations will have to await kinetic analysis of the wild type and judiciously prepared mutants.

Our investigations also show that the release of iron from *Pa* FtnA and *Pa* BfrB has different regulatory needs (Figure 7). To place these observations in context, it is important to note that iron replete conditions cause strong positive regulation of a *bfrB* gene, whereas iron limitation causes its negative regulation.[40] Iron limitation also causes a strong positive regulation of the *bfd* and *fpr* genes,[41] which encode a bacterioferritin-associated ferredoxin and a ferredoxin nicotinamide adenine dinucleotide phosphate reductase, respectively,[54] suggesting that the Bfd and Fpr proteins are involved in the process of release of iron from BfrB.[22] Reconstitution of *Pa* BfrB with *Pa* Fpr in vitro causes the iron mineral to be mobilized slowly (black trace in the plot of Scheme 1A). In contrast, reconstitution of *Pa* BfrB with *Pa* Fpr and apo *Pa* Bfd causes significant acceleration of iron release, as indicated by the red trace. These observations were interpreted to indicate that *Pa* FPR mediates the flow of electrons from NADPH to the mineral in *Pa* BfrB via the heme and that interactions between apo *Pa* Bfd and *Pa* BfrB promote the

Scheme 1. Distinct Requirements for the Release of Iron Stored in *Pa* BfrB and *Pa* FtnA

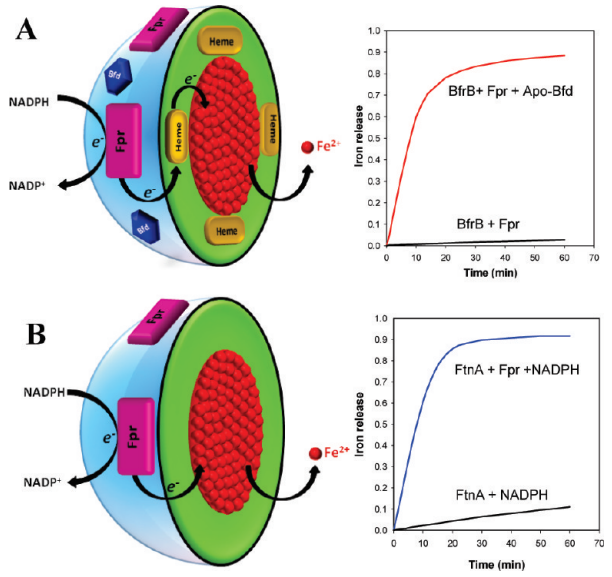

release of iron from *Pa* BfrB (Scheme 1A).[22] Similar experiments with *Pa* FtnA reveal important differences in the processes of iron release between the two ferritin-like molecules in *P. aeruginosa*. Addition of NADPH to a solution of *Pa* FtnA reconstituted with only *Pa* Fpr is sufficient to cause rapid release of iron stored in *Pa* FtnA (blue trace in Scheme 1B). Similar experiments in the presence of apo *Pa* Bfd do not have an appreciable effect on the rate of iron release (Figure 7A), which indicates that only electrons from a suitable donor can cause efficient mobilization of iron stored in *Pa* FtnA. These contrasting observations add strong support to the notion that *Pa* FtnA and *Pa* BfrB are two distinct ferritins in *P. aeruginosa*.

■ ASSOCIATED CONTENT

Supporting Information. Amino acid sequence of the protein encoded by the *P. aeruginosa bfrA* gene (*Pa* FtnA) aligned against the amino acid sequences of bacterioferritins of known structure, $2F_o - F_c$ electron density maps of the ferroxidase center ligands of *Pa* FtnA Fe soaked and doubly soaked, conformational changes in the *Pa* FtnA ferroxidase center upon binding iron, and anomalous difference map showing sulfate in a three-fold pore. This material is available free of charge via the Internet at http://pubs.acs.org.

Accession Codes

Coordinates and crystallographic structure factors for the distinct *Pa* FtnA structures have been deposited in the Protein Data Bank as entries 3R2O (as isolated at pH 6.0), 3R2K (as isolated at pH 7.5), 3R2H (as isolated at pH 10.5), 3R2R (Fe-soaked at pH 6.0), 3R2L (Fe-soaked at pH 7.5), 3R2S (doubly soaked at pH 6.0), and 3R2M (doubly soaked at pH 7.5).

■ AUTHOR INFORMATION

Corresponding Author

*Ralph N. Adams Institute for Bioanalytical Chemistry and Department of Chemistry, University of Kansas, Multidisciplinary Research Building, 2030 Becker Dr., Lawrence, KS 66047. Telephone: (785) 864-4936. Fax: (785) 864-1916. E-mail: mrivera@ku.edu.

Funding Sources

This work was supported by grants from the National Science Foundation (MCB-0818488), the National Institute of Health (GM-50503), and the National Center for Research Resources (P20 RR-17708).

■ ACKNOWLEDGMENT

The assistance of Mr. Ritesh Kumar in the preparation of Scheme 1 is acknowledged. Use of IMCA-CAT beamline 17-BM and 17-ID at the Advanced Photon Source was supported by the companies of the Industrial Macromolecular Crystallography Association through a contract with the Hauptaman-Woodward Medical Research Institute. Use of the Advanced Photon Source was supported by the U.S. Department of Energy, Office of Science, Office of Basic Energy Sciences, under Contract DE-AC02-06CH11357.

■ REFERENCES

(1) Köster, W. (2001) ABC Transporter-Mediated Uptake of Iron, Siderophores, Heme and Vitaming B_{12}. *Res. Microbiol. 152*, 291–301.

(2) Byers, B. R., and Arcenaux, J. E. L. (1998) Microbial Iron Transport: Iron Acquisition by Pathogenic Mircroorganisms. In *Metal Ions in Biological Systems* (Sigel, A., Sigel, H., and Sigel, R., Eds.) Plenum Press, New York.

(3) Wandersman, C., and Stojiljkovic, I. (2000) Bacterial Heme Sources: The Role of Heme, Hemoprotein Receptors and Hemophores. *Curr. Opin. Microbiol. 3*, 215–220.

(4) Genco, C. A., and Dixon, D. W. (2001) Emerging Strategies in Microbial Haem Capture. *Mol. Microbiol. 39*, 1–11.

(5) Andrews, S. C. (1998) Iron Storage in Bacteria. *Adv. Microb. Physiol. 40*, 281–351.

(6) Smith, L. (2004) The Physiological Role of Ferritin-Like Compounds in Bacteria. *Crit. Rev. Microbiol. 30*, 173–185.

(7) Ilari, A., Stefanini, S., Chiancone, E., and Tsernoglou, D. (2000) The Dodecameri Ferritin from *Listeria innocua* Contains a Novel Intersubunit Iron-Binding Site. *Nat. Struct. Biol. 7*, 38–43.

(8) Keyer, K., and Imlay, J. A. (1996) Superoxide Accelerates DNA-Damage by Elevating Free-Iron Levels. *Proc. Natl. Acad. Sci. U.S.A. 193*, 13635–13649.

(9) Ma, J.-F., Ochsner, U. A., Klotz, M. G., Nanayakkara, V. K., Howell, M. L., Johnson, Z., Posey, J. E., Vasil, M. L., Monaco, J. J., and Hassett, D. J. (1999) Bacterioferritin A Modulates Catalase A (KatA) Activity and Resistance to Hydrogen Peroxide in *Pseudomonas aeruginosa*. *J. Bacteriol. 181*, 3730–3742.

(10) Escolar, L., Perez-Martin, J., and De Lorenzo, V. (1999) Opening the Iron Box: Transcriptional Metalloregulation by the Fur Protein. *J. Bacteriol. 181*, 6223–6229.

(11) Ochsner, U. A., and Vasil, M. L. (1996) Gene Repression by the Ferric Uptake Regulator in *Pseudomonas aeruginosa*: Cycle Selection of Iron Regulated Genes. *Proc. Natl. Acad. Sci. U.S.A. 93*, 4409–4414.

(12) Wilderman, P. J., Sowa, N. A., FitzGerald, D. J., FitGerald, P. C., Gottesman, S., Ochsner, U. A., and Vasil, M. L. (2004) Identification of Tandem Duplicate Regulatory Small RNAs in *Pseudomonas aeruginosa* Involved in Iron Homeostasis. *Proc. Natl. Acad. Sci. U.S.A. 101*, 9792–9797.

(13) Wilks, A., and Burkhard, K. A. (2007) Heme and Virulence: How Bacterial Pathogens Regulate, Transport and Utilize Heme. *Nat. Prod. Rep. 24*, 511–522.

(14) Cornelis, P., Matthijs, S., and Van Oeffelen, L. (2009) Iron Uptake Regulation in *Pseudomonas aeruginosa*. *BioMetals 22*, 15–22.

(15) Wyckoff, E., Boulette, M. L., and Payne, S. M. (2009) Genetics and Environmental Regulation of *Shigella* Iron Transport Systems. *BioMetals 22*, 43–51.

(16) Cornelissen, C. N., and Sparling, P. F. (1994) Iron Piracy: Acquisition of Transferrin-Bound Iron by Bacterial Pathogens. *Mol. Microbiol. 14*, 843–850.

(17) Vasil, M. L., and Ochsner, U. A. (1999) The Response of *Pseudomonas aeruginosa* to Iron: Genetics, Biochemistry and Virulence. *Mol. Microbiol. 34*, 399–413.

(18) Vasil, M. L. (2007) How We Learnt About Iron Acquisition in *Pseudomonas aeruginosa*: A Series of Very Fortunate Events. *BioMetals 20*, 587–601.

(19) Liu, X., and Theil, E. C. (2005) Ferritins: Dynamic Management of Biological Iron and Oxygen Chemistry. *Acc. Chem. Res. 38*, 167–175.

(20) Andrews, S. C. (2010) The Ferritin-Like Superfamily: Evolution of the Biological Iron Storeman from a Rubrerythrin-Like Ancestor. *Biochim. Biophys. Acta 1800*, 691–705.

(21) Le Brun, N. E., Crow, A., Murphy, M. E. P., Mauk, A. G., and Moore, G. R. (2010) Iron Core Mineralization in Prokaryotic Ferritins. *Biochim. Biophys. Acta 1800*, 732–744.

(22) Weeratunga, S., Gee, C. E., Lovell, S., Zeng, Y., Woodin, C. L., and Rivera, M. (2009) Binding of *Pseudomonas aeruginosa* Apobacterioferritin-Associated Ferredoxin to Bacterioferritin B Promotes Heme Mediation of Electron Delivery and Mobilization of Core Mineral Iron. *Biochemistry 48*, 7420–7431.

(23) Andrews, S. C. (2010) The Ferritin-like Superfamily: Evolution of the Biological Iron Storeman from a Ruberythrin-Like Ancestor. *Biochim. Biophys. Acta 1800*, 691–705.

(24) Weeratunga, S., Lovell, S., Yao, H., Battaile, K. P., Fischer, C. J., Gee, C. E., and Rivera, M. (2010) Structural Studies of Bacterioferritin B (BfrB) from *Pseudomonas aeruginosa* Suggest a Gating Mechanism for Iron Uptake via the Ferroxidase Center. *Biochemistry 49*, 1160–1175.

(25) Crow, A., Lawson, T. L., Lewin, A., Moore, G. R., and Le Brun, N. E. (2009) Structural Basis for Iron Mineralization by Bacterioferritin. *J. Am. Chem. Soc. 131*, 6808–6813.

(26) Swartz, L., Kuchinskas, M., Li, H., Poulos, T. L., and Lanzilotta, W. N. (2006) Redox-Dependent Structural Changes in the *Azotobacter vinelandii* Bacterioferritin: New Insights into the Ferroxidase and Iron Transport Mechanism. *Biochemistry 45*, 4421–4428.

(27) Macedo, S., Romão, C. V., Mitchell, E., Matias, P. M., Liu, M. Y., Xavier, A. V., LeGall, J., Teixeira, M., Lindley, P., and Carrondo, M. A. (2003) The Nature of the Di-Iron Site in the Bacterioferritin from *Desulfovibrio desulfuricans*. *Nat. Struct. Biol. 10*, 285–290.

(28) Janowski, R., Auerbach-Nevo, T., and Weiss, M. S. (2007) Bacterioferritin from *Mycobacterium smegmatis* Contains Zinc in its Di-Nuclear Site. *Protein Sci. 17*, 1138–1150.

(29) Stillman, T. J., Hempstead, P. D., Artymiuk, P. J., Andrews, S. C., Hudson, A. J., Treffry, J. R., Guest, P. M., and Harrison, P. M. (2001) The High-Resolution X-ray Crystallographic Structure of the Ferritin (EcFtnA) of *Escherichia coli*; comparison with human H Ferritin (HuHF) and the Structures of the Fe^{3+} and Zn^{2+} Derivatives. *J. Mol. Biol. 307*, 587–603.

(30) Cho, K. J., Shin, H. J., Lee, J.-H., Kim, K.-J., Park, S. S., Lee, Y., Lee, C., Park, S. S., and Kim, K. H. (2009) The Crystal Structure of Ferritin from *Helicobacter pylori* Reveals Unusual Conformational Changes for Iron Uptake. *J. Mol. Biol. 390*, 83–98.

(31) Tatur, J., Hagen, W. R., and Matias, P. M. (2007) Crystal Structure of the Ferritin from the Hyperthermophilic Archaeal Anaerobic *Pyrococcus furiosus*. *J. Biol. Inorg. Chem. 12*, 615–630.

(32) Johnson, E., Cascio, D., Sawaya, M. R., Gingery, M., and Schroder, I. (2005) Crystal Structures of a Tetrahedral Open Pore Ferritin from the Hyperthermophilic Archaeon *Archaeoglobus fulgidus*. *Structure 13*, 637–648.

(33) Treffry, A., Zhao, Z., Qail, M. A., Guest, J. R., and Harrison, P. M. (1998) How the Presence of Three Iron Binding Sites Affects the Iron Storage Function of the Ferritin (EcFtnA) of *Escherichia coli*. *FEBS Lett. 432*, 213–218.

(34) Moore, G. R., Mann, S., and Bannister, J. V. (1986) Isolation and Properties of the Complex Nonheme-Iron-Containing Cytochrome b_{557} (Bacterioferritin) from *Pseudomonas aeruginosa*. *J. Inorg. Biochem. 28*, 329–336.

(35) Moore, G. R., Kadir, H. A., Al-Massad, K., Le Brun, N. E., Thomson, A. J., Greenwood, C., Keen, J. N., and Findlay, J. B. C. (1994) Structural Heterogeneity of *Pseudomonas aeruginosa* Bacterioferritin. *Biochem. J. 304*, 493–497.

(36) Andrews, S. C., Harrison, P. M., and Guest, J. R. (1989) Cloning, Sequencing, and Mapping of the Bacterioferritin Gene (*bfr*) of *Escherichia coli* K-12. *J. Bacteriol. 171*, 3940–3947.

(37) Garg, R. P., Vargo, C. J., Cui, X., and Kurtz, D. M. J. (1996) A [2Fe-2S] Protein Encoded by an Open Reading Frame Upstream of the *Escherichia coli* Bacterioferritin Gene. *Biochemistry 35*, 6297–6301.

(38) Quail, M. A., Jordan, P., Grogan, J. M., Butt, J. N., Lutz, M., Thomson, A. J., Andrews, S. C., and Guest, J. R. (1996) Spectroscopic and Voltammetric Characterization of Bacterioferritin-Associated Ferredoxin of *Escherichia coli*. *Biochem. Biophys. Res. Commun. 229*, 635–642.

(39) Stover, C. K., Pham, X. Q., Erwin, A. L., Mizoguchi, S. D., Warrener, P., Hickey, M. J., Brinkman, F. S. L., Hufnagle, W. O., Kowalik, D. J., Lagrou, M., Garber, R. L., Goltry, L., Tolentino, E., Westbrock-Wadman, S., Yuan, Y., Brody, L. L., Coulter, S. N., Folger, K. R., Kas, A., Larbig, K., Lim, R., Simith, K., Spencer, D., Wong, G. K. S., Wu, Z., Paulsen, I. T., Reizer, J., Saler, M. H., Hancock, R. E. W., Lory, S., and Olson, M. V. (2000) Complete Genome Sequence of *Pseudomonas aeruginosa* PA01, an Opportunistic Pathogen. *Nature 406*, 959–964.

(40) Palma, M., Worgall, S., and Quadri, L. E. N. (2003) Transcriptome Analysis of the *Pseudomonas aeruginosa* Response to Iron. *Arch. Microbiol. 180*, 374–379.

(41) Ochsner, U. A., Wilderman, P. J., Vasil, A. I., and Vasil, M. L. (2002) GeneChip Expression Analysis of the Iron Starvation Response in *Pseudomonas Aeruginosa*: Identification of Novel Pyoverdine Biosynthesis Genes. *Mol. Microbiol. 45*, 1277–1287.

(42) Ikemura, T. (1985) Codon Usage and tRNA Content in Unicellular and Multicellular Organisms. *Mol. Biol. Evol. 2*, 13–34.

(43) Ringeling, P. L., Davy, S. L., Monkara, F. A., Hunt, C., Dickson, D. P. E., McEwan, A. G., and Moore, G. R. (1994) Characterization of Bacterioferritin and Formation of Non-Haem Iron Particles in Intact Cells. *Eur. J. Biochem. 223*, 847–855.

(44) Otwinowski, Z., and Minor, W. (1997) Processing of X-ray Diffraction Data Collected in Oscillation Mode. *Methods Enzymol. 276*, 307–326.

(45) Kabsch, W. (1988) Automatic indexing of rotation diffraction patterns. *J. Appl. Crystallogr. 21*, 67–72.

(46) Evans, P. (2006) Scaling and assessment of data quality. *Acta Crystallogr. D62*, 72–82.

(47) Vagin, A., and Teplyakov, A. (1997) *MOLREP*: An Automated Program for Molecular Replacement. *J. Appl. Crystallogr. 30*, 1022–1025.

(48) Adams, P. D., Afonine, P. V., Brunkózci, G., Chen, V. B., Davis, I. W., Echols, N., Headd, J. J., Hung, L.-W., Kapral, G. J., Grosse-Kunstleve, R. W., McCoy, A. J., Moriarty, N. W., Oeffner, R., Read, R. J., Richardson, D. C., Richardson, J. S., Terwilliger, T. C., and Zwart, P. H. (2010) PHENIX: A Comprehensive Python-Based System for Macromolecular Structure Solution. *Acta Crystallogr.D66*, 213–221.

(49) Emsley, P., and Cowtan, K. (2004) Coot: Model-building tools for molecular graphics. *Acta Crystallogr. D60*, 2126–2132.

(50) Lovell, S. C., Davis, I. W., Arendall, W. B., III, de Bakker, P. I., Word, J. M., Prisant, M. G., Richardson, J. S., and Richardson, D. S. (2003) Structure Validation by Cα Geometry: ϕ,ψ and Cβ Deviation. *Proteins 30*, 437–450.

(51) Chen, V. B., Arendall, W. B., III, Headd, J. J., Keedy, D. A., Immormino, R. M., Kapral, G. J., Murray, L. W., Richardson, J. S., and Richardson, D. C. (2010) MolProbity: All-Atom Structure Validation for Macromolecular Crystallography. *Acta Crystallogr. D66*, 12–21.

(52) Kurtz, D. M. (1997) Stuctural Similarity and Functional Diversity of Diiron-Oxo Proteins. *J. Biol. Inorg. Chem. 2*, 159–167.

(53) Liu, H.-L., Zhou, H.-N., Xing, W.-M., Zhao, J.-F., Li, S.-X., Huang, J.-F., and Bi, R.-C. (2004) 2.6 Å Resolution Crystal

Structure of the Bacterioferritin from *Azotobacter vinelandii*. *FEBS Lett.* *573*, 93–98.

(54) Wang, A., Zeng, Y., Han, H., Weeratunga, S., Morgan, B. N., Moënne-Loccoz, P., Schönbrunn, E., and Rivera, M. (2007) Biochemical and Structural Characterization of *Pseudomonas aeruginosa* Bfd and FPR: Ferredoxin $NADP^+$ Reductase and Not Ferredoxin is the Redox Partner of Heme Oxygenase under Iron-Starvation Conditions. *Biochemistry* *46*, 12198–12211.

(55) Diederichs, K., and Karplus, P. A. (1997) Improved R-factors for Diffraction Data Analysis in Macromolecular Crystallography. *Nat. Struct. Biol.* *4*, 269–275.

(56) Lawson, D. M., Artymiuk, P. J., Yewdall, S. J., Smith, J. A., Livingstone, J. C., Treffry, A., Luzzago, A., Levi, S., Arosio, P., Cesareni, G., Thomas, C. D., Shaw, W. V., and Harrison, P. M. (1991) Solving the Structure of Human H Ferritin by Genetically Engineering Intermolecular Crystal Contacts. *Nature* *349*, 541–544.